Monthly Notices
of the
ROYAL ASTRONOMICAL SOCIETY

MNRAS **469,** S459–S474 (2017) doi:10.1093/mnras/stx2018

Evolution of the physical properties of dust and cometary dust activity from 67P/Churyumov–Gerasimenko measured *in situ* by *Rosetta*/COSIMA

Sihane Merouane,[1⋆] Oliver Stenzel,[1⋆] Martin Hilchenbach,[1⋆] Rita Schulz,[2] Nicolas Altobelli,[3] Henning Fischer,[1] Klaus Hornung,[4] Jochen Kissel,[1] Yves Langevin,[5] Eva Mellado,[4] Jouni Rynö[6] and Boris Zaprudin[7]

[1]*Max-Planck-Institut für Sonnensystemforschung, Justus-von-Liebig-Weg 3, D-37077, Göttingen, Germany*
[2]*European Space Agency, PO Box 299, NL-2200 AG, Noordwijk, The Netherlands*
[3]*Solar System Science Operation Division, ESA-ESAC, PO Box 78, E-28691 Villanueva de la Cañada, Madrid, Spain*
[4]*Universität der Bundeswehr München, LRT-7, D-85577 Neubiberg, Germany*
[5]*Institut d'Astrophysique Spatiale, CNRS/Université Paris-Sud, Bâtiment 121, F-91405 Orsay, France*
[6]*Finnish Meteorological Institute, Erik Palmenin aukio 1, PO Box 503, FI-00101 Helsinki, Finland*
[7]*Tuorla Observatory, Department of Physics and Astronomy, University of Turku, Väisäläntie 20, FI-21500 Piikkiö, Finland*

Accepted 2017 August 3. Received 2017 July 31; in original form 2017 April 21

ABSTRACT

The Cometary Secondary Ion Mass Analyzer (COSIMA) collects dust particles in the coma of 67P/Churyumov–Gerasimenko, images them with a resolution of 14 μm × 14 μm, and measures their composition via time-of-flight secondary ion mass spectrometry. The particles are collected on targets exposed to the cometary flux for periods ranging from several hours to a week. Images are acquired with the internal camera, the COSISCOPE, before and after each exposure period. This paper focuses on the evolution of the dust flux and of the size distribution of the particles derived from the COSISCOPE images during the two years of the mission. The dust flux reaches its maximum at perihelion. We suggest that the delay of 20 d between the activity measured by COSIMA and the gas activity measured by the other instruments on *Rosetta* is caused by the presence of a volatile-poor dust layer on the nucleus that is removed around perihelion, uncovering volatile-rich layers that then become active. The difference in morphology between the northern and southern hemispheres observed by OSIRIS, the south being more sintered, is also recorded in the COSIMA data by a change in the size distribution during the southern summer, as the large porous aggregates disappear from the COSIMA collection. The properties of the particles collected during an outburst in early September 2016 indicate that these particles were ejected by a violent event and might originate from regions of low tensile strength.

Key words: comet: 67P/Churyumov-Gerasimenko.

1 INTRODUCTION

The Cometary Secondary Ion Mass Analyzer (COSIMA), located on the *Rosetta* orbiter, is an instrument dedicated to the collection of dust particles in the coma of comet 67P/Churyumov–Gerasimenko (67P hereafter), to their imaging via an internal camera and to the measurement of their composition via time-of-flight secondary ion mass spectrometry (TOF-SIMS) (Kissel et al. 2007). The fact that the dust particles are collected at very low velocities (Rotundi et al. 2015; Della Corte et al. 2015) means that they suffer very little damage on collection; thus their physical properties can be studied in an unprecedented state of preservation.

The physical properties of the dust particles collected by COSIMA were investigated during the first six months of the *Rosetta* mission at the comet, while the comet was at distances greater than 2 au from the Sun. Langevin et al. (2016) described the morphology of the particles. Two main types of particles are collected: clusters of particles that fragment upon impact on the COSIMA plates (themselves classified into three categories: the rubble piles, the shattered clusters and the glued clusters) and unfragmented particles, termed 'compact' in the Langevin classification. Hornung et al. (2016) used the fragmentation patterns to assess the tensile strength

⋆ E-mail: merouane@mps.mpg.de (SM); stenzel@mps.mpg.de (OS); hilchenbach@mps.mpg.de (MH)

of the cometary dust particles collected by COSIMA and derived a strength of the order of magnitude of 1 kPa. The particle size distribution as well as the dust flux, which is related to the cometary dust activity, were explored by Merouane et al. (2016). The dust activity observed at distances from 3.5 to 1.9 au from the Sun increases with a power law that is consistent with remote observations of 67P activity from its previous perihelion passages.

In order to understand what drives the cometary dust activity, it is essential to measure the activity of comets along their trajectory around the Sun. Before the *Rosetta* mission, the only measurements of comet activity possible for extended periods of time were those via remote observations, and mainly from ground-based telescopes. Several observations of 67P around its perihelion have been performed from Earth (Fulle et al. 2004; Agarwal, Müller & Grün 2007; Fulle et al. 2010; Snodgrass et al. 2013). These observations show a peak in the photometric data at about 15 to 20 d after the perihelion. Such a shift in time of the recorded dust activity has also been reported for several other comets (Ferrín 2005). The interpretation of the photometric data has to take into account the size distribution of the dust particles, in particular because it appears to change with the seasons, becoming steeper when the comet approaches perihelion (Fulle et al. 2004). It is thus very important to characterize the dust properties from new data acquired *in situ* in order to obtain constraints for future dust modelling and ground-based data interpretation.

In the present paper, we focus on the evolution of the particle flux and of the particle size distribution measured for the entire two years of the *Rosetta* mission at the comet; that is, from 3.55 au to perihelion, and from perihelion to 3.8 au.

2 METHODS

2.1 Dust particle collection and imaging

The COSIMA collecting targets consist of 1 cm × 1 cm plates covered with various metals (Hornung et al. 2014). The targets are mounted on holders, each of which contains three of these targets. The target holder exposed to the cometary dust flux is located at the end of a 16-cm-long dust funnel with an aperture of 15° × 23°. During the Rosetta mission, seven target holders were exposed. The time-resolved exposure periods lasted from a few hours up to 3 weeks, a given target holder being used several times until the coverage of one of its targets reached about 1 per cent. Before the first exposure and after each exposure period, images of each target were acquired with the internal microscope camera of COSIMA, named COSISCOPE. This camera images the dust particles with a resolution of 14 μm × 14 μm. A detailed description of the COSISCOPE subsystem can be found in Kissel et al. (2007) and in Langevin et al. (2016).

In order to image the particles, two LEDs illuminate the target holder, one on each side of the holder, with a grazing incidence of about 5°. The grazing incidence allows the detection of the dust particles by their brightness when the particles are brighter than the target material, and/or by their shadows. In order to spot the new particles collected after a given exposure period, the images acquired prior to and after the exposure are blinked, and the positions of the new particles on the target as well as their areas are determined.

2.2 Flux determination

The mass flux of the particles can be calculated by measuring the volume of cometary material collected and assuming some value for the density. The area measured from the COSISCOPE image gives an estimate for the particle radius, assuming that the particles are circular. In order to account for the possible flattening of the particles upon impact on the targets, half-spheres are used to calculate their volume. The error bars on the volume are calculated from the two following extreme cases for the particle shapes: they are assumed to be spherical for the upper limit, and cylindrical with a thickness of the order of magnitude of the COSISCOPE resolution, namely 14 μm, for the lower limit.

The mass is determined using a fit to the particle densities derived in Hornung et al. (2016) for particles up to 30 μm in size:

$$\rho = \rho_0 \, (r/r_0)^{-\log 2.5}, \tag{1}$$

with $r_0 = 1$ μm and $\rho_0 = 1000\,\mathrm{kg\,m^{-3}}$. This relationship implies that a 100-nm particle would have a density of 2500 $\mathrm{kg\,m^{-3}}$, and a 15-μm particle a density of 340 $\mathrm{kg\,m^{-3}}$. Larger particles are assumed to be composed of subelements with a 15-μm radius, a 50 per cent filling factor and a density of 170 $\mathrm{kg\,m^{-3}}$. These densities take into account only the refractory part of the particles, as the temperature inside the instrument is of the order of 10°C. The density of dust particles mixed with ices would be higher, as the voids are filled and the porosity decreased.

2.3 Fragmentation in the instrument

As the target holder is located at the back-end of the dust funnel, the incoming dust particles are likely to hit the walls of the funnel and are potentially fragmented before being collected on the COSIMA targets. Several bursts of dust particles have been observed within COSIMA, and in these cases the particles are located mainly in a specific area of the target holder, thus showing a clear non-random spatial distribution (Merouane et al. 2016, fig. 2). In order to determine the flux of dust particles and the size distribution, possible fragmentation in the funnel is taken into account by analysing the spatial distribution of the dust particles on the target holder. The method, described in detail in Merouane et al. (2016), consists of comparing the observed spatial distribution for a given exposure period with one million randomly generated distributions of the same number of particles. If the observed distribution cannot be reproduced more than a certain percentage of times, such as 5 per cent, 3 per cent or 1 per cent, the distribution is likely to be non-random and is assumed to be the result of a single parent-particle impact on the funnel walls. The size of that parent particle is estimated by adding the volumes of all daughter particles and assuming that the initial particle was spherical. The fragmentation inside the funnel and the possible rebounding of particles off the target imply that the flux derived in this paper constitutes a lower limit of the dust flux.

In order to measure the dust flux per unit area, the cross-section of the instrument, taking into account the possibility of fragmentation on the funnel walls, has to be determined. The funnel is 16 cm long, with two inclined walls, and has an entrance area of 4 cm × 6 cm (see the detailed description of the instrument in Kissel et al. 2007). If the dust enters the funnel close to its entrance, it is likely to hit one of the walls and bounce several times until reaching one of the targets. The more encounters a given particle has with the funnel walls, the more probable it is to stick to the funnel and not reach the target holder. In order to estimate the height of the funnel under which particle collection is optimum, we performed numerical simulations of dust particles entering the COSIMA funnel with a normal incidence angle to the target-holder plane. In the simulation, 620 particles enter the funnel at a random position at its entrance. Only particles that end up on one of the targets after suffering not more than a

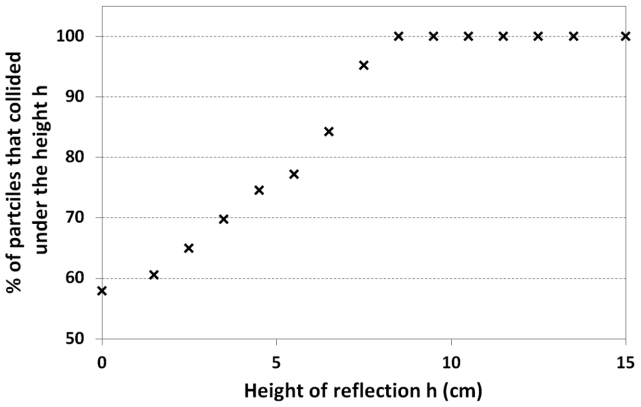

Figure 1. Percentage of particles in the numerical simulation that end up on the target plate that were reflected from the funnel wall at a height lower than h. The target holder is at height zero.

single collision are considered to be collected. For each particle ending on one of the three targets, the height of collision with the funnel wall is recorded. When a particle hits the target without colliding with the funnel, this height is equal to zero. Fig. 1 shows, for each height of collision in the funnel noted h, the percentage of particles collected on the target holder that hit the funnel at a height smaller than h. In total, 58 per cent of the particles that were collected on the holder did not hit the funnel wall before hitting the target. None of the particles collected on the target collided with the funnel wall more than 8–9 cm above the target holder. We thus use the area of the funnel at this height, which is 18 cm^2, to calculate the flux of dust particles.

3 RESULTS

During the two years of the mission, seven sets of targets were exposed to the cometary dust flux, and 731 d of COSIMA operations were dedicated to the collection of dust particles, which corresponds to about 74 per cent of the whole mission; the remainder of the operation time was devoted to the imaging and chemical analysis of the collected particles. Table 1 summarizes the exposure periods of each target holder and their dust coverage. The total number of particles and fragments of particles collected during the whole mission reached 35 191. Among the 346 collection periods, 83 were associated with fragmentation events. When taking these events into account, the amount of parent particles estimated is between 1216 and 1621. This implies that between 33 570 and 33 975 particles detected on the COSIMA targets are associated with fragmentation events, which corresponds to 95 to 97 per cent of the total number of particles detected.

It can be seen from Table 1 that most of the particles tend to be collected on the top and middle targets of the holders. There are at least two possible explanations for this bias. (1) Because the dust particles are very slow, of the order of magnitude of the spacecraft velocity (Rotundi et al. 2015; Della Corte et al. 2015), there is a strong aberration in the direction of motion of the particles with respect to the COSIMA target plane when the particles enter the instrument. This could lead to an increased incidence angle of the particles in the funnel and so to their collection in a preferred location of the target holder. (2) The spacecraft and instrument potentials around COSIMA might cause the charged dust particles to be deflected (Fulle et al. 2015), also leading to an increased incidence angle of the particles entering COSIMA.

If only one target holder had been exposed during the whole mission, as illustrated in Fig. 2, the resultant coverage would be 11.2 per cent. The bias towards the top and middle targets can clearly be seen in this figure. For each of these targets, four regions close to the corners show a lack of particles. These positions correspond to the positions of the screws with which the targets are mounted on the holder. Because the screws are at a slightly different height from the target surface, they are slightly out of focus, and this results in a lower detection efficiency, which explains the low amount of dust in these particular places. Two targets made of plane silver were used for collection, among the 21 targets exposed during the whole *Rosetta* mission. They did not show a lower collection efficiency compared with the more porous material used for the other targets, which was intended to be more 'sticky' (Hornung et al. 2014). We can thus exclude the possibility that the lack of detection on the screws is a result of their surface being too smooth for particles to stick to.

The evolution of the volume of cometary material collected during the whole mission and of the number of particles is shown in Fig. 3(a) and (b). The heliocentric and nucelocentric distances (c and d), the latitude (e) and the phase angle (f) are also shown. The number of particle fragments, the estimated number of parent particles, as well as the corresponding volume of material are summarized in Table A1 in Appendix A. The large vertical steps in the evolution of the volume with time correspond to a large amount of material collected in very short time periods (typically a day). In most cases, these collections are associated with the fragmentation of a large single parent in the dust funnel, and hence the evolution of the number of parent particles shows less variation than the evolution of the number of daughter particles.

In order to analyse the evolution of the dust flux with the heliocentric distance, it is essential to take into account the evolution of

Table 1. The start of the first exposure period and the end of the last exposure period for each target holder. The fourth column gives the range of heliocentric distances crossed during that time period. The last four columns indicate the dust coverage of the three targets (top, middle and bottom) of each holder as well as the total coverage (top+middle+bottom targets).

Target holder	Start of the first exposure	End of the last exposure	Range of heliocentric distances [au]	Top target	Middle target	Bottom target	Total coverage
D0	2014-08-11	2014-12-12	3.57 - 2.78 inbound	0.5 per cent	0.7 per cent	1.3 per cent	0.9 per cent
CF	2014-12-16	2015-02-09	2.76 - 2.36 inbound	1.8 per cent	3.5 per cent	0.6 per cent	1.9 per cent
C7	2015-02-14	2015-04-06	2.32 - 1.92 inbound	4.8 per cent	0.3 per cent	1.1 per cent	2.1 per cent
D1	2015-04-10	2015-05-27	1.89 - 1.55 inbound	1.2 per cent	4.6 per cent	1.1 per cent	2.3 per cent
CD	2015-05-30	2015-10-07	1.53 in - 1.41 out	3.5 per cent	1.0 per cent	0.3 per cent	1.6 per cent
D2	2015-10-11	2016-05-08	1.43 - 2.96 outbound	0.8 per cent	0.8 per cent	0.08 per cent	0.6 per cent
C3	2016-05-10	2016-09-27	2.98 - 3.81 outbound	2.6 per cent	2.0 per cent	0.8 per cent	1.8 per cent
All	2014-08-11	2016-09-27	3.57 in - 3.81 out	15.3 per cent	12.9 per cent	5.3 per cent	11.2 per cent

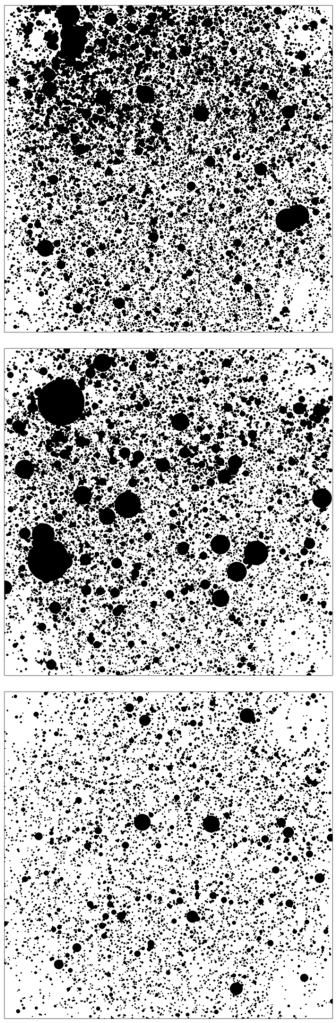

Figure 2. Sum of all the particles collected as if a single target holder had been exposed. The size of each target is 1 cm × 1 cm. Each dot represents a single dust particle collected, with the dot area corresponding to the particle area.

the dust flux with respect to the comet distance. As was shown in Merouane et al. (2016), no fragmentation between 10 and 300 km was observed by COSIMA; the dust evolution with the comet distance can thus be modelled by a $1/distance^2_{\rm comet}$ law. We applied this law to normalize the data at a distance of 10 km from the comet centre and plot the evolution of the flux with respect to the heliocentric distance in Fig. 4. As the COSIMA fluxes show variations on very short time-scales (Merouane et al. 2016), the data are averaged in heliocentric distance bins of 0.5 au in order to smooth these local variations and focus on the large-scale evolution of the cometary activity. The flux is also represented in volume (Fig. 4b) and in mass (Fig. 4c) using the size–density relationship given in equation (1).

The maximum flux is observed at perihelion if the flux is expressed in terms of the number of particles, but before perihelion if the flux is expressed in terms of volume (or mass). This implies that the particles collected before perihelion are much larger than the ones collected after perihelion (see the more detailed discussion on the size distribution in Section 4.2).

The flux of dust particles varies with the heliocentric distance but also with the local time on the comet nucleus at which the particles are collected. Fig. 5 shows the flux of dust with respect to the subspacecraft latitude and local time. Each panel represents

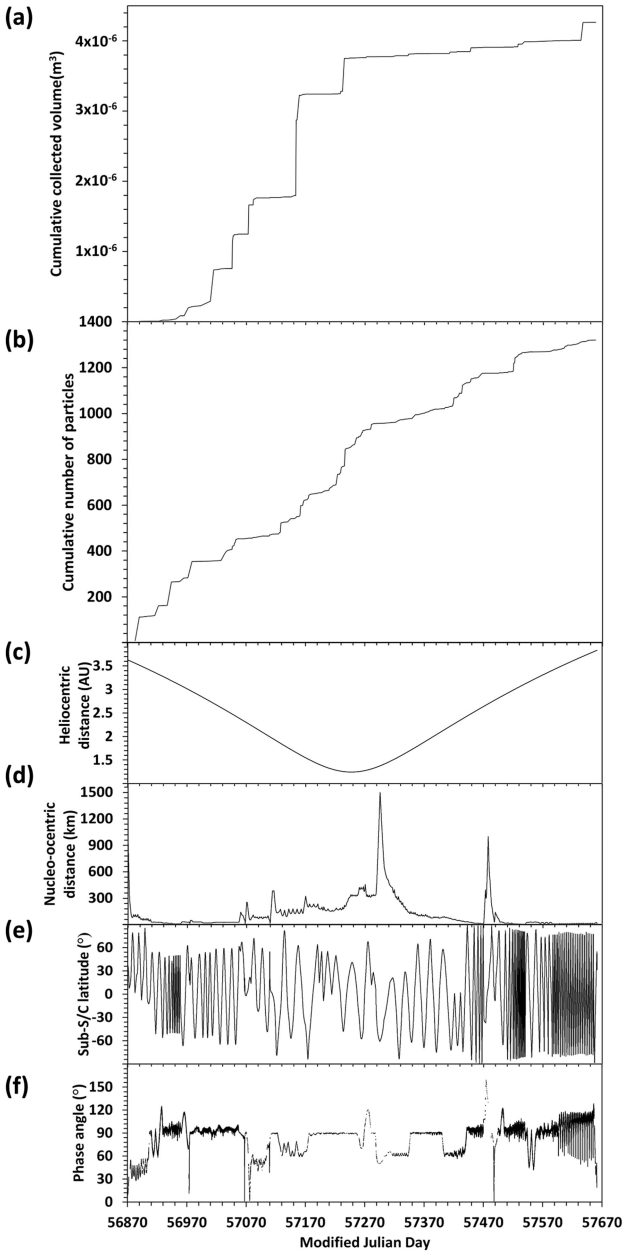

Figure 3. (a) Cumulative volume of cometary material collected during the course of the mission. (b) Cumulative estimated number of parent particles collected during the course of the mission. (c) Heliocentric distance. (d) Distance from *Rosetta* to the centre of the nucleus. (e) Subspacecraft latitude. (f) Phase angle.

a different season. The red empty dots show the collection periods during which no particles were collected.

The size distributions of the dust particles measured throughout the *Rosetta* mission are shown in Fig. 6. In each panel, the cumulative power index α measured for particles in the range of 30 to 150 μm in diameter is indicated. At sizes smaller than 30 μm, the detection of particles is biased as their size reaches the limit of detection of COSIMA. In order to estimate this bias, we compared the total size distributions with that of Ligier et al. (2017), which used an automatic detection method. We estimate the underestimation of the 1- and 2-pixel-area particles to be a factor of 4 and of 1.3, respectively. We applied this correction to our data in Fig. 6,

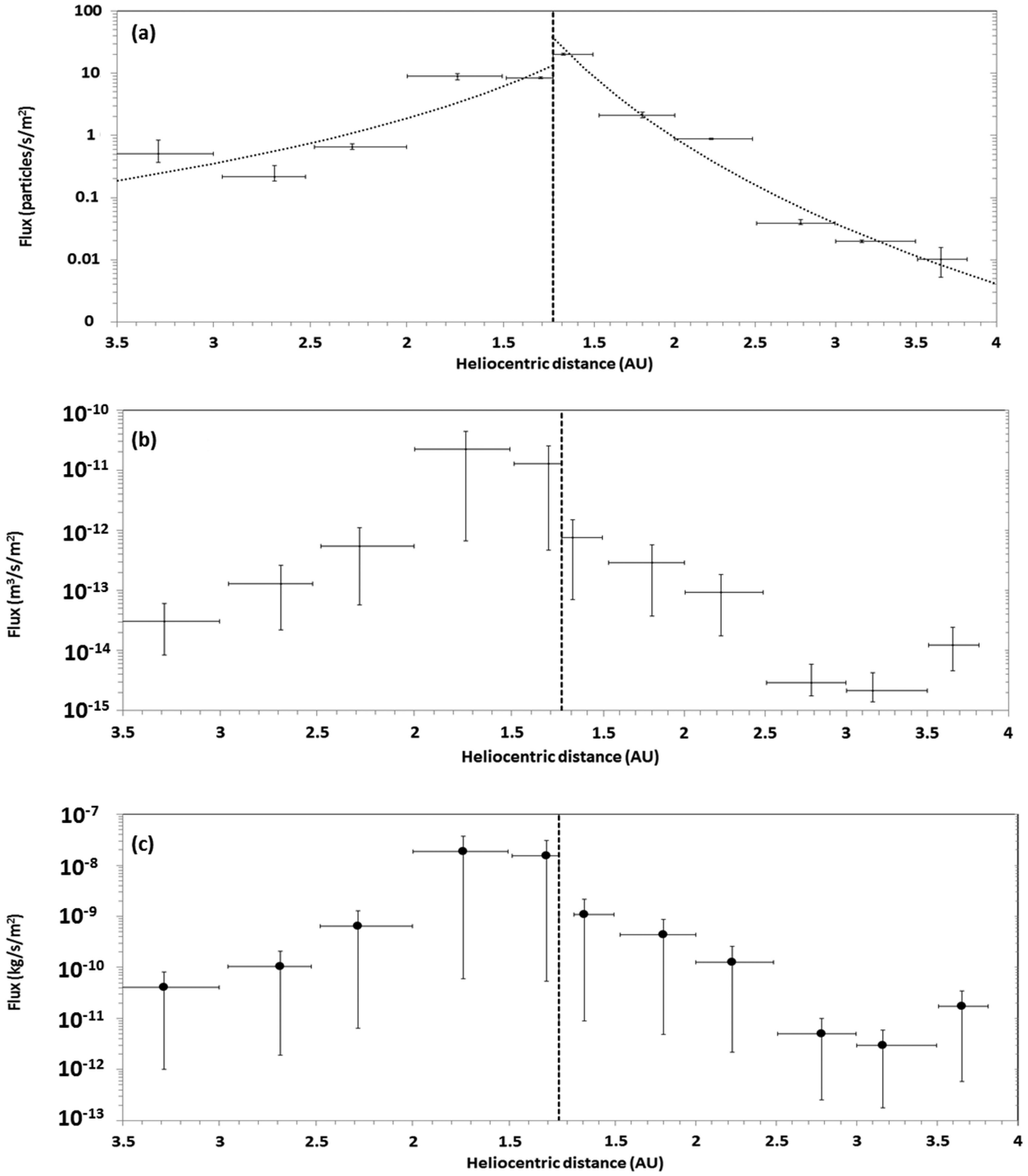

Figure 4. Evolution of the flux of dust collected with respect to the heliocentric distance. The fluxes are normalized to a distance of 10 km from the comet centre and averaged in heliocentric distance bins of 0.5 au. The perihelion is shown by the dashed line. Flux expressed (a) in number, (b) in volume, (c) in mass using equation (1) (Hornung et al. 2016).

as shown by the open circles. The most notable change in the size distribution of the particles before and after the perihelion passage is the decrease of very large particles after perihelion. Only one large particle (larger than 500 μm in diameter) was collected in the year after perihelion, this particle being collected during an outburst event (for more details see Section 4.3).

During the terrestrial summer of 2015, several outbursts were observed by the OSIRIS camera system as well as by the navigation camera NAVCAM (Vincent et al. 2016). Outbursts differ from jet-like features by their very short duration and intense nature. For the *in situ* dust instruments, the detection of an outburst is a challenge, as the dust flux can be highly variable over time periods of a day. With a time resolution of a few minutes, the detection of outbursts might be feasible, but with a longer time resolution (typically a day to a week), only the convergence of observations by several instruments of the dust flux allow such an interpretation. The first

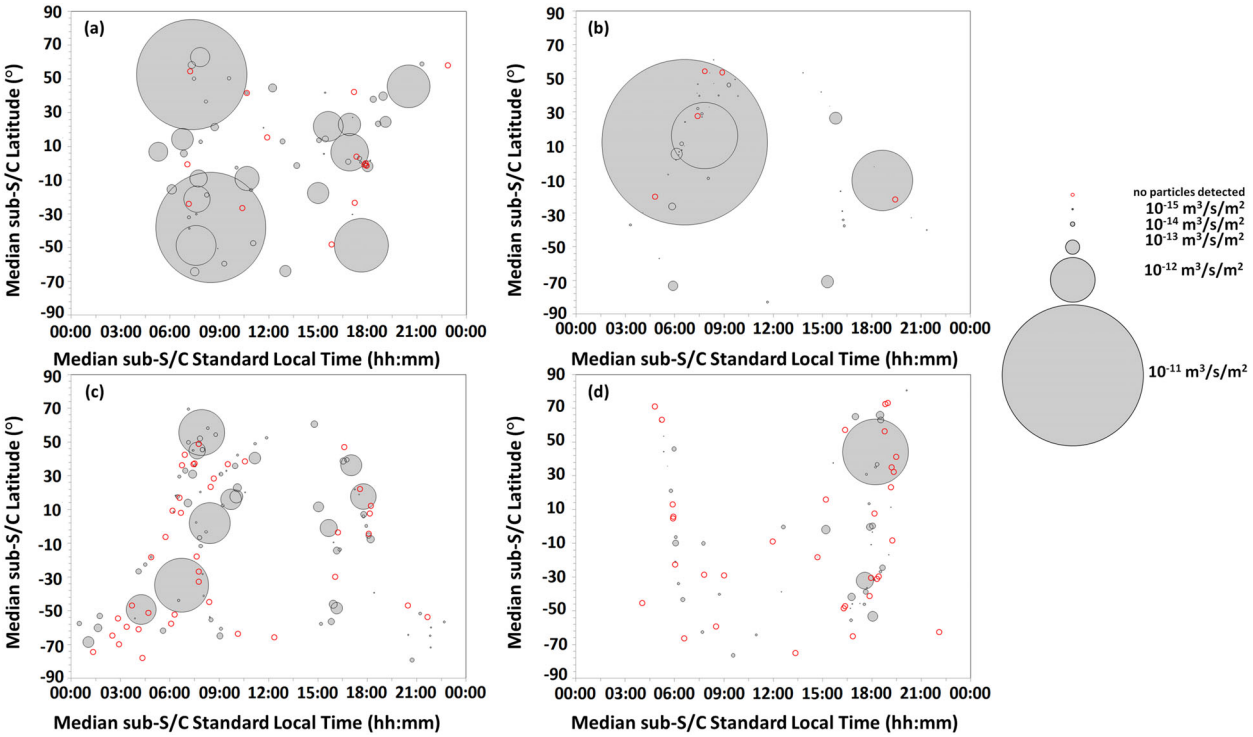

Figure 5. Volume flux of dust particles with respect to the subspacecraft latitude and local time. The size of the dots is proportional to the volume flux. The empty red dots show the collection periods during which no particles were collected. Panel (a) shows the data acquired between 2014 August and the equinox of 2015 May, panel (b) between the equinox and the perihelion, panel (c) between the perihelion and the equinox of 2016 April, and panel (d) between the equinox and end of 2016 September.

outburst detected by several instruments of the orbiter occurred on 2016 February 19. Grün et al. (2016) reported the detection of a dust cloud by the camera system OSIRIS, followed by an increase in both the dust and the gas activity measured at the spacecraft. COSIMA did not record any data on that day, as the instrument was not in exposure mode but was acquiring the mass spectra of dust particles. However, two other events detected by several instruments have been recorded by COSIMA: one on 2016 July 3 (Agarwal et al., in revision) and one on 2016 September 5. The COSISCOPE images taken before and after this last event are shown in Fig. 7.

The exposure of the target holder started on 2016 September 5 at 05:20 UTC and ended on September 6 at 07:17 UTC. During this exposure, 5223 particles were collected. As can be seen in the images, the bottom target is much less crowded by dust than the top and middle targets. Our analysis of the spatial distribution of the particles on the target holder for this exposure suggests that the particles are not randomly distributed, and the distribution is thus considered to be the result of a unique parent particle of estimated size about 500 μm fragmenting in the funnel. However, the coverage of the top and middle targets is quite high and well distributed. No other events with coverage this good have been observed to date during similar fragmentation events of similar-sized parent particles. It is possible that more than one large particle has entered the funnel and fragmented inside it.

4 DISCUSSION

4.1 Evolution of the cometary dust activity

The total estimated mass of dust collected during the two years of the *Rosetta* mission is 0.22 mg using the size–density relationship of equation (1); or, using a constant density of 1000 kg m^{-3}, the total mass would be 1.28 mg. The last column of Table 1 shows an increase of the dust coverage until the perihelion in 2015 August followed by a decrease, consistent with an increase in dust activity as the comet approaches the Sun and a decrease while the comet moves away from the Sun. A high dust coverage is observed for the last target holder exposed (holder C3) compared with the previous one (holder D2), which is a result of an outburst that occurred between 2016 September 5 and 6, which alone represents 74 per cent of all the particles collected on this target holder (see Section 4.3). The maximum of the dust activity measured by COSIMA occurs at perihelion and drops considerably by one order of magnitude after the perihelion passage.

The slopes of the power laws that describe the increase in cometary activity while the comet approaches the Sun and its decrease after the perihelion passage are quite different. The power index measured before perihelion is -4.1 ± 0.5, whereas it is -7.8 ± 0.4 after perihelion. Several power indices have been determined from ground-based observations of previous perihelion passages of 67P, depending mainly on the models used for the dust properties: −5.08 (Agarwal et al. 2007) measured for both in and outbound, −3 (Ishiguro 2008) measured pre-perihelion. The upper and lower limits of the dust mass-loss rates are estimated in Fulle et al. (2010) for distances ranging from 3.4 to 1.3 au before perihelion. From their tables 3 and 4, we find that the mass-loss rate that they calculate evolves with the heliocentric distance with a power index of between −6 and −7, which is steeper than the above values. Boehnhardt et al. (2016) measured the decrease in dust activity from ground-based observations of 67P after the 2015 perihelion passage. They report a power index ranging from −3.73 to −4.21, depending on the dust phase function model used, for

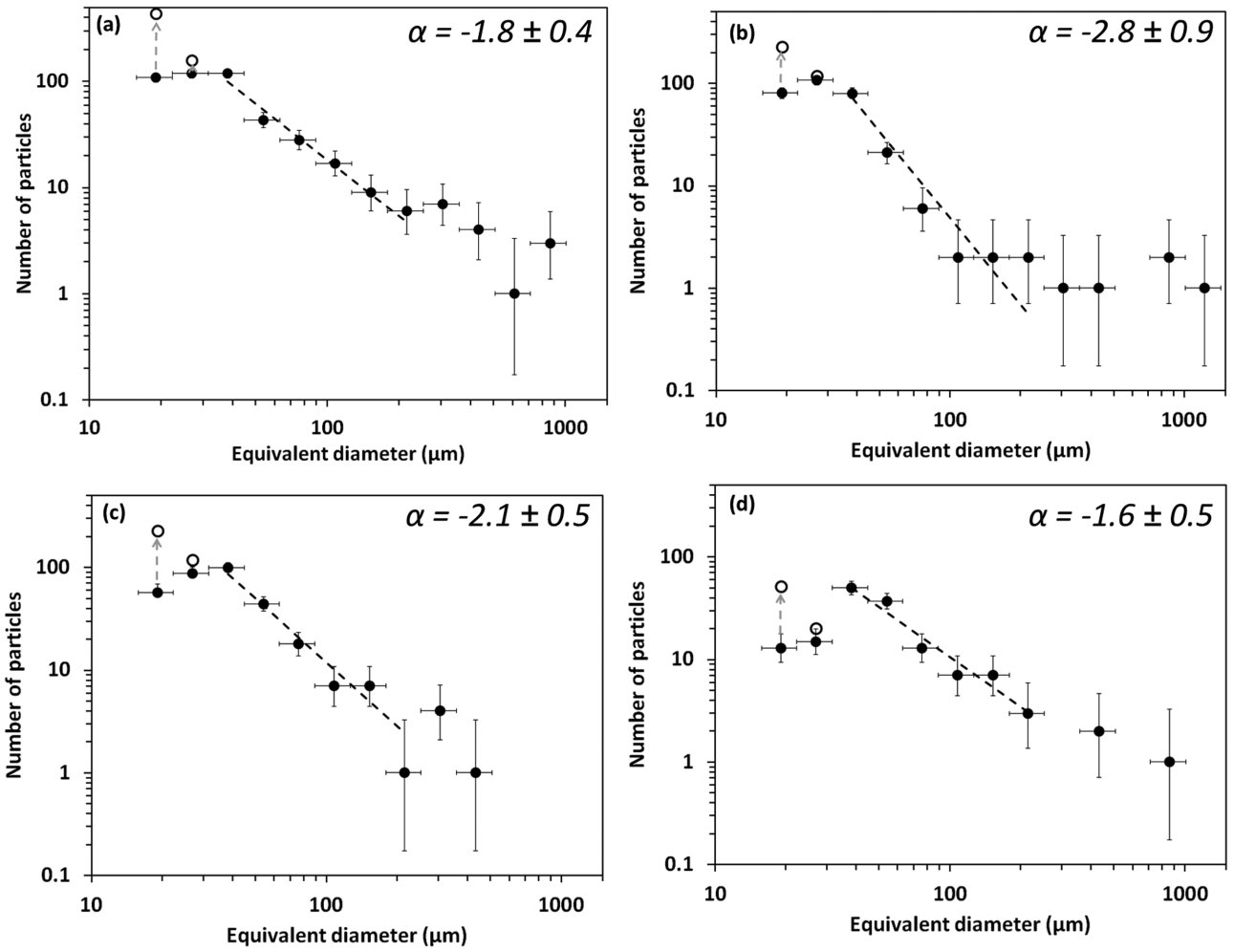

Figure 6. Size distributions measured (a) between 2014 August and the 2015 May equinox, (b) between the equinox and the perihelion, (c) between the perihelion and the 2016 April equinox, and (d) between the equinox and the end of 2016 September. The dashed lines are the best fits for the size distribution of the particles in the 30- to 150-μm size range. The corresponding power index is given in each panel. The open circles indicate the number of particles adjusted for the observation bias (for details see text).

heliocentric distances ranging from 1.2482 to 2.9663 au. Schulz, Stüwe & Boehnhardt (2004) observed a strong decrease in the dust activity by a factor of 21 between 2.3 and 2.9 au outbound between 2003 February and June. The data from their table 1 show that the dust activity decreases with a power index of about −13. This value is much steeper than the other observations reported above.

We can compare the COSIMA data with the observations made *in situ* by the other instruments on *Rosetta*. The power index measured pre-perihelion by COSIMA implies an increase in the production rate slightly lower than that measured by the GIADA instrument (Della Corte et al. 2015), which reports an increase by a factor of 6 in the dust production rate from 3.36 to 2.43 au, while our power law implies an increase by a factor of about 4 in the same period. The difference could arise from the data selection. Della Corte et al. (2015) compared the data at the two heliocentric distances for a similar phase angle and latitudes. Because the exposure times of COSIMA are too long to enable the selection of a specific set of latitudes, we used all the data available in our set. The flux of dust can be influenced by the pointing: when the spacecraft is pointing away from the nucleus (for example to map the coma), there is a lower probability of collecting dust, which might lower the value of our dust fluxes. Because these periods are short during our exposure windows, however, the influence of such parameters is not dramatic. A multi-instrument analysis of both the water production rate and the dust production rate (Hansen et al. 2016) shows an asymmetry in the comet activity around perihelion. The power index derived before perihelion is -5.18 ± 0.006 using data from ROSINA, VIRTIS, RPC and MIRO, or -5.10 ± 0.05 using ROSINA data only; this index decreases to -7.15 ± 0.08 after perihelion using ROSINA data. These values are closer to the ones measured by COSIMA compared with the power indices derived from ground-based observations.

The *in situ* measurements of the gas activity (Bockelée-Morvan et al. 2016; Fougere et al. 2016) show that the gas activity of 67P reaches its maximum between 15 and 20 d after perihelion. The activity measured by COSIMA shows a maximum exactly at perihelion if the focus is on the number of particles collected (Fig. 4a), and 3 to 4 months before perihelion if the focus is on the volume (or mass) of particles collected (Fig. 4b and c). We suggest that

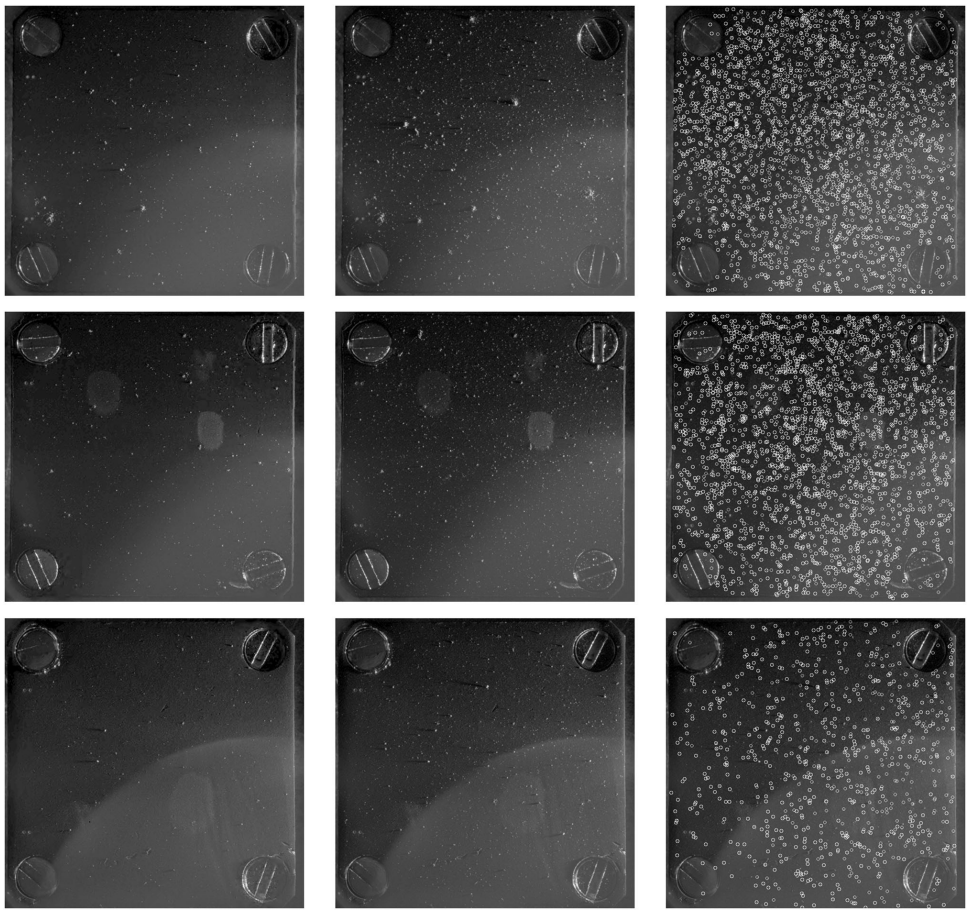

Figure 7. COSISCOPE images taken before the outburst of 2016 September 5 (left column) and after the outburst (central column). The top, middle and bottom rows show the top, middle and bottom targets, respectively. The right column highlights the position of the particles collected during the outburst with white circles. The size of each target is 1 cm × 1 cm.

this delay between the maximum of the dust activity and of the gas activity, both measured *in situ*, is the result of the presence of a layer of dust with a very low volatile content at the surface of the comet that needs to be lifted off to uncover the more volatile-rich layers, which, once exposed to solar illumination, become active. Fornasier et al. (2016) also suggest that the ice is located beneath a thin layer of dust in order to explain the colour variation of the 67P nucleus over time.

The time resolution of the COSIMA exposures allows us to measure the evolution of the dust flux with the local time under the spacecraft, as this parameter is usually stable over extended periods of time. In Fig. 5, each panel represents a different season on the comet: (a) from 2014 August to the equinox of 2015 May, (b) from the equinox to perihelion, (c) from perihelion to the equinox of 2016, and (d) after the equinox. In all cases, these plots show that the volume of dust particles collected is usually higher in the morning than in the evening. This indicates that the material collected on the morning side of the terminator has a higher volatile content than that on the evening side. These volatile materials are accumulated during the night, and start to outgas when illuminated by the Sun. On the evening side, the material has been illuminated all day and thus might contain fewer volatiles, as most of them should have been lost by the time the spacecraft flies above. The ejection of dust particles is thus more efficient in the morning than in the evening, resulting in a larger collection of dust at the spacecraft when it flies above the morning side of the terminator.

4.2 Evolution of the dust size distribution

From the beginning of the *Rosetta* mission in 2014 August to the equinox in 2015 May, the cumulative power index derived is −1.8 (Fig. 6a). Later on, from the equinox to the perihelion, the size distribution becomes steeper and the cumulative power index reaches −2.8 (Fig. 6b) This power index stays close to this value (−2.1) until the next equinox in 2016 April (Fig. 6c). After the equinox until the end of the *Rosetta* mission in 2016 September, the power index reaches a value of −1.6 (Fig. 6d), which is close to the value measured at the beginning of the mission. The size distribution observed around perihelion compared with the size distribution observed before and after the equinoxes tends to show that large particles are associated with the northern hemisphere. This might reflect differences in the nature of the terrains in the northern and southern hemispheres of the comet. From the optical images of the OSIRIS camera onboard *Rosetta*, the nucleus shows a dichotomy in terms of morphology between the northern and southern hemispheres (El-Maarry et al. 2016). While the northern hemisphere shows large areas of smooth terrain covered with dust, the southern hemisphere appears more consolidated, with several regions

presenting long fractures, suggesting a sintered material. The particles collected by COSIMA during the northern summer might originate from the smooth large terrains, while the particles collected during the southern summer could originate from fractures.

It is also notable that the very large particles (larger than 500 μm) almost disappear from the COSIMA collection after the equinox. A decrease in the number of large particles (larger than about 100 μm) is also observed from the GIADA instrument onboard *Rosetta*: this instrument observed a change in the power index of the cumulative size distribution from −1.0 before the 2015 May equinox to −2.7 after the equinox for this size of particle (Fulle et al. 2016).

At sizes smaller than 30 μm, it can be seen that the lack of very small particles is significant after perihelion after correction from the detection bias (open circles in Fig. 6). Because the cometary particles are charged (Fulle et al. 2015), it is possible that these particles are decelerated, deviated or even repelled as they approach the charged spacecraft. These particles can become negatively charged by electrons in the coma plasma. If we assume a charge of about −10 V (of the order of the spacecraft potential) and size-dependent particle velocities (Agarwal et al. 2007), particles smaller than 10 μm cannot hit the spacecraft. Because the potential of the spacecraft varies with time (Odelstad et al. 2015), it is still possible to collect small particles, but with a modulation in time.

We investigated how the size distribution potentially changes with the solar irradiation encountered by the dust particles in the coma. We estimated, for each collection period, the solar irradiance at the distance from the Sun where the particles were collected and multiplied this by the travel time of the particle from the comet to *Rosetta* using a velocity of 3 ms^{-1}, consistent with GIADA measurements (Della Corte et al. 2015). The scatter plot showing the size of the particles with respect to their exposure to the solar irradiance is shown in Fig. 8(a). The power indices determined from these distributions are shown in panel (b). If the particles fragment or sinter owing to ice loss on their way to the spacecraft, a change in the size distribution with respect to the amount of energy that they receive from the Sun might be expected. The range of sizes as well as the corresponding power index measured by COSIMA do not show any significant changes. No evidence is thus found for particles fragmenting or sintering during their trajectory from the nucleus to the spacecraft over distances ranging from 10 to 300 km.

4.3 Outbursts

The particles collected during the September outburst are very similar in terms of morphology to the particles collected during the rest of the mission. The four typologies defined in Langevin et al. (2016) (rubble piles, shattered clusters, glued clusters and compact particles) can be seen during this single event. The main difference between the particles from this event and the particles that are not associated with an outburst is the size distribution of the fragments on the targets. The size distribution can be fitted by a power law with a cumulative index of −3.0. This can be compared with previous analyses of the fragmentation patterns of the particles collected by COSIMA (Hornung et al. 2016), in which a value of -2.3 ± 0.2 was determined. Two parameters influence the size distribution of the fragments created by the impact of one or several parent particles. The first is the impact velocity of the particles. The faster they impact the target, the easier it is for them to be fragmented, because the energy upon impact is higher. A steep size distribution indicates that the particles that were collected during that event might be

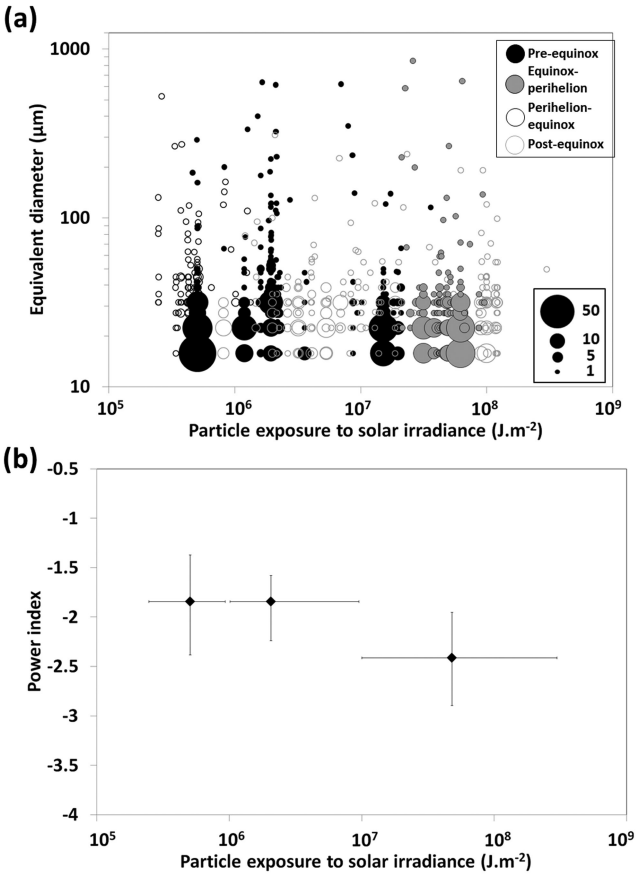

Figure 8. (a) The sizes of the particles in each collection period with respect to the energy received by the Sun. The size of the dots is proportional to the number of particles in each size bin. (b) The corresponding power indices. The error bars are statistical error bars (1σ).

faster than the particles collected in the weeks around this event and that are not associated with outbursts. This implies that the process that releases the particles during outbursts must be a violent one that can accelerate dust particles faster than the sublimation of ice on the surface. The second parameter that can influence the size distribution of fragments upon impact on the COSIMA target is the tensile strength of the particles. It is easier to break up a particle into its smaller constituents if it has a low tensile strength. The fact that the size distribution of the fragments during the outburst is steep implies that the incoming particle(s) should have a low tensile strength, or at least lower than the values derived in Hornung et al. (2016) of 1 kPa.

5 CONCLUSIONS

We analysed the evolution of the dust flux and of the size distribution of the particles collected by COSIMA onboard *Rosetta* during the whole course of the mission, from 3.55 au to perihelion and from perihelion to 3.8 au. The cometary dust activity observed by COSIMA does not coincide with the maximum of activity measured by the gas instruments onboard *Rosetta* (ROSINA and MIRO). We suggest that this is because the high-volatile layers on the nucleus are covered by a low-volatile layer of dust that needs to be removed before then high-volatile layers are exposed.

The size distribution of the particles that are likely to come from the northern hemisphere differs from that of the particles that are

likely to come from the southern hemisphere. These latter particles have a steeper size distribution and do not exhibit a large amount of aggregates in the 0.1- to 1-mm size range, in contrast to the particles coming from the northern side. We suggest that the large aggregates collected by COSIMA originate from the smooth dust-covered areas observed by OSIRIS in the northern hemisphere.

COSIMA recorded two outbursts during the mission jointly with other instruments. The last outburst recorded, at about 3.7 au from the Sun, was particularly intense, with the largest collection ever recorded by COSIMA, comprising more than 5000 particles and particle fragments in one day. The data analysis of this particular event shows that the number of parent particles that entered the instrument might be lower, as they probably fragmented on the walls of the funnel. The sizes of the fragments lead us to conclude that the speed of the particles might have been high and/or the tensile strength of these particles might be low, suggesting either a violent event at the origin of this outburst, and/or that the particles ejected during this event might come from a region of lower tensile strength, perhaps located under the more sintered surface of the nucleus.

ACKNOWLEDGEMENTS

COSIMA was built by a consortium led by the Max-Planck-Institut für Extraterrestrische Physik, Garching, Germany in collaboration with Laboratoire de Physique et Chimie de l'Environnement et de l'Espace, Orléans, France; the Institut d'Astrophysique Spatiale, CNRS/Université Paris Sud, Orsay, France; the Finnish Meteorological Institute, Helsinki, Finland; the Universität Wuppertal, Wuppertal, Germany; von Hoerner und Sulger GmbH, Schwetzingen, Germany; the Universität der Bundeswehr, Neubiberg, Germany; the Institut für Physik, Forschungszentrum Seibersdorf, Seibersdorf, Austria; and the Space Research Institute, Austrian Academy of Sciences, Graz, Austria. It is led by the Max-Planck-Institut für Sonnensystemforschung, Göttingen, Germany. The support of the national funding agencies of Germany (DLR, grant 50 QP 1302), France (CNES), Austria, Finland and the ESA Technical Directorate is gratefully acknowledged. We thank the Rosetta Science Ground Segment at ESAC, the Rosetta Mission Operations Centre at ESOC and the Rosetta Project at ESTEC for their outstanding work that has enabled the Science return of the *Rosetta* Mission. *Rosetta* is an ESA mission with contributions from its member states and NASA.

REFERENCES

Agarwal J., Müller M., Grün E., 2007, Space Sci. Rev., 128, 79
Bockelée-Morvan D. et al., 2016, MNRAS, 462, 170
Boehnhardt H., Riffeser A., Kluge M., Ries C., Schmidt M., Hopp U., 2016, MNRAS, 462, 376
Della Corte V. et al., 2015, A&A, 26208
El-Maarry M. R. et al., 2016, A&A, 593, 110
Ferrín I., 2005, Icarus, 178, 493
Fornasier S. et al., 2016, Science, 354, 1566
Fougere N. et al., 2016, MNRAS, 462, 156
Fulle M., Barbieri C., Cremonese G., Rauer H., Weiler M., Milani G., Ligustri R., 2004, A&A, 422, 357
Fulle M. et al., 2010, A&A, 522, 63
Fulle M. et al., 2015, ApJ, 802, L12
Fulle M. et al., 2016, ApJ, 821, 19
Grün E. et al., 2016, MNRAS, 462, 220
Hansen K. C. et al., 2016, MNRAS, 462, 491
Hornung K. et al., 2014, Planet. Space Sci., 103, 309
Hornung K. et al., 2016, Planet. Space Sci., 133, 63
Ishiguro M., 2008, Icarus, 193, 96
Kissel J. et al., 2007, Space Sci. Rev., 128, 823
Langevin Y. et al., 2016, Icarus, 271, 76
Ligier N., Langevin Y., Hilchenbach M., Merouane S., Cosima Team, 2017, in Lunar and Planetary Science Conference. LPI Contribution No. 1964, p. 2166
Merouane S. et al., 2016, A&A, 596, 87
Odelstad E. et al., 2015, Geophys. Res. Lett., 42, 10
Rotundi A. et al., 2015, Science, 347, 3905
Schulz R., Stüwe J. A., Boehnhardt H., 2004, A&A, 422, L19
Snodgrass C., Tubiana C., Bramich D. M., Meech K., Boehnhardt H., Barrera L., 2013, A&A, 557, 33
Vincent J.-B. et al., 2016, MNRAS, 462, 184

APPENDIX A: NUMBER AND VOLUME OF PARTICLES COLLECTED

Table A1. For each collection period: start and end of the exposure periods, number of fragments of particles detected on the target holder, estimated number of parent particles, and volume of material collected assuming a half-sphere shape.

Start date (YYYY-MM-DDThh:mm:ss)	End date (YYYY-MM-DDThh:mm:ss)	Number of fragments	Number of parents (3 per cent level of confidence)	Volume (m^3)
2014-08-11T09:00:40	2014-08-17T18:34:12	9	9	1.51E-10
2014-08-18T02:11:34	2014-08-24T18:49:13	103	103	3.66E-09
2014-08-25T02:34:35	2014-08-29T18:49:12	9	1	3.17E-09
2014-09-02T09:33:24	2014-09-05T07:19:12	2	2	6.88E-12
2014-09-05T15:21:31	2014-09-12T11:30:11	34	1	7.98E-10
2014-09-13T12:06:32	2014-09-19T07:19:12	2	2	1.95E-11
2014-09-19T16:27:14	2014-09-25T06:49:12	43	43	8.42E-10
2014-09-25T16:26:34	2014-10-03T18:49:10	72	1	1.40E-08
2014-10-04T04:01:30	2014-10-10T18:49:11	130	1	4.96E-10
2014-10-11T04:05:23	2014-10-17T18:49:12	102	102	6.25E-09
2014-10-18T04:03:04	2014-10-24T18:49:11	176	1	1.11E-08
2014-10-25T10:58:52	2014-10-31T06:49:12	560	1	4.28E-08
2014-10-31T20:56:17	2014-11-07T07:19:11	15	15	1.37E-09
2014-11-07T17:44:47	2014-11-14T07:19:12	741	1	1.13E-07
2014-11-14T11:38:24	2014-11-21T08:49:13	71	71	1.84E-08
2014-11-21T14:06:33	2014-12-12T15:10:22	199	1	9.91E-09
2014-12-16T13:06:33	2014-12-20T06:01:31	1872	1	6.52E-08
2014-12-20T11:55:00	2014-12-27T02:32:16	1582	1	4.49E-07
2014-12-27T07:08:36	2015-01-02T06:46:23	64	1	1.58E-09
2015-01-02T11:22:43	2015-01-09T03:50:54	238	1	1.16E-08
2015-01-09T08:27:16	2015-01-14T04:15:14	28	28	3.71E-09
2015-01-14T06:10:18	2015-01-15T07:16:40	12	12	3.35E-10
2015-01-15T09:11:42	2015-01-20T02:00:10	4	4	8.60E-11
2015-01-23T12:41:32	2015-01-24T04:15:14	4	4	5.23E-11
2015-01-24T06:10:06	2015-01-24T20:31:33	1709	1	4.03E-07
2015-01-25T08:44:33	2015-01-26T02:56:48	12	12	1.32E-09
2015-01-26T04:57:02	2015-01-27T04:12:37	136	1	5.96E-08
2015-01-27T06:12:55	2015-01-28T04:15:16	16	1	3.11E-10
2015-01-28T06:15:42	2015-01-29T07:16:40	133	1	2.12E-08
2015-01-29T09:17:30	2015-01-30T03:50:57	12	12	3.01E-10
2015-01-30T05:51:45	2015-01-31T04:15:14	3	3	2.48E-11
2015-01-31T06:16:10	2015-02-01T06:44:10	12	12	2.86E-10
2015-02-01T08:44:58	2015-02-02T04:15:15	1	1	1.79E-11
2015-02-02T06:16:17	2015-02-03T04:12:36	1	1	9.29E-11
2015-02-03T06:13:28	2015-02-09T10:05:12	134	1	4.79E-09
2015-02-14T09:37:15	2015-02-14T15:45:55	0	0	0
2015-02-14T22:07:15	2015-02-15T02:45:11	0	0	0
2015-02-15T05:21:31	2015-02-15T12:30:12	0	0	0
2015-02-15T14:51:32	2015-02-16T00:00:12	0	0	0
2015-02-16T02:36:32	2015-02-16T12:00:10	1	1	3.85E-11
2015-02-16T14:36:33	2015-02-18T17:30:13	0	0	0
2015-02-18T21:21:33	2015-02-19T01:30:13	0	0	0
2015-02-19T06:06:33	2015-02-19T13:15:11	1	1	5.06E-11
2015-02-19T17:06:33	2015-02-20T10:00:11	0	0	0
2015-02-20T23:06:30	2015-02-21T11:02:10	0	0	0
2015-02-22T11:21:31	2015-02-27T04:34:10	3609	1	4.16E-07
2015-02-27T08:53:14	2015-02-27T12:45:10	0	0	0
2015-02-27T14:51:31	2015-02-27T17:45:11	0	0	0
2015-02-27T19:33:31	2015-02-27T22:30:11	0	0	0
2015-02-28T00:18:31	2015-02-28T13:15:11	1	1	2.75E-11
2015-02-28T15:21:32	2015-02-28T19:15:12	1	1	1.79E-11
2015-03-01T20:36:31	2015-03-09T09:11:15	1885	1	7.53E-08
2015-03-13T06:22:53	2015-03-19T07:05:56	712	1	2.28E-08
2015-03-19T09:33:24	2015-03-20T03:33:05	5	5	1.32E-10
2015-03-20T06:00:39	2015-03-23T02:43:39	0	0	0
2015-03-23T05:11:07	2015-03-24T08:54:44	0	0	0
2015-03-24T11:22:10	2015-03-27T13:10:14	0	0	0
2015-03-27T14:12:02	2015-03-27T17:40:14	0	0	0
2015-03-27T18:42:14	2015-03-27T22:35:14	0	0	0
2015-03-27T23:37:06	2015-03-28T06:13:15	0	0	0
2015-03-28T07:15:05	2015-03-28T12:25:15	2	2	6.03E-11
2015-03-28T13:27:09	2015-03-28T18:00:13	66	1	2.11E-09

Table A1 – *continued*

Start date (YYYY-MM-DDThh:mm:ss)	End date (YYYY-MM-DDThh:mm:ss)	Number of fragments	Number of parents (3 per cent level of confidence)	Volume (m^3)
2015-03-28T19:01:59	2015-03-28T21:00:15	1	1	6.37E-11
2015-03-28T22:02:03	2015-04-06T03:07:38	67	1	2.70E-09
2015-04-10T19:44:55	2015-04-11T06:07:51	3	3	5.51E-11
2015-04-11T16:34:44	2015-04-13T02:48:35	6	1	1.95E-10
2015-04-14T04:09:56	2015-04-15T02:35:15	0	0	0
2015-04-15T04:21:29	2015-04-16T07:05:56	7	7	1.94E-10
2015-04-16T08:52:06	2015-04-17T03:33:05	201	1	4.70E-09
2015-04-17T05:22:07	2015-04-20T02:43:39	41	41	9.94E-10
2015-04-20T04:30:37	2015-04-21T08:54:43	1	1	2.75E-11
2015-04-21T10:41:31	2015-04-26T02:15:16	92	1	3.09E-09
2015-04-26T13:56:53	2015-04-29T15:56:20	24	1	5.06E-10
2015-05-01T05:50:42	2015-05-02T04:15:15	9	1	1.90E-10
2015-05-02T06:02:01	2015-05-03T16:44:56	14	14	1.34E-10
2015-05-07T18:24:15	2015-05-09T20:42:35	720	1	2.07E-08
2015-05-09T22:31:33	2015-05-10T16:49:57	1	1	9.73E-12
2015-05-10T18:38:53	2015-05-11T12:57:20	1	1	2.63E-10
2015-05-11T14:46:06	2015-05-12T09:04:41	2849	1	1.08E-06
2015-05-12T11:06:31	2015-05-13T16:04:54	5	5	1.06E-10
2015-05-16T13:18:43	2015-05-17T16:49:57	1255	1	3.51E-07
2015-05-17T18:55:27	2015-05-18T12:57:20	3	3	4.55E-11
2015-05-18T15:02:48	2015-05-19T09:04:41	3	3	5.85E-11
2015-05-19T11:10:05	2015-05-20T05:52:02	41	41	6.04E-10
2015-05-22T19:33:36	2015-05-24T05:54:19	175	1	1.38E-08
2015-05-24T07:59:49	2015-05-25T11:13:26	18	18	2.05E-10
2015-05-25T13:19:06	2015-05-26T06:46:11	4	4	1.00E-10
2015-05-26T08:52:07	2015-05-27T12:05:12	93	1	1.88E-09
2015-05-30T04:04:35	2015-05-31T06:44:41	2	2	2.75E-11
2015-05-31T08:27:11	2015-06-01T02:51:02	3	3	5.51E-11
2015-06-01T04:33:24	2015-06-02T09:00:29	3	3	4.07E-11
2015-06-02T10:42:45	2015-06-03T06:00:12	14	14	1.63E-10
2015-06-05T15:40:52	2015-06-07T06:44:42	4	4	1.14E-10
2015-06-07T08:26:58	2015-06-12T08:36:20	1	1	9.73E-12
2015-06-14T02:26:13	2015-06-15T07:00:15	2	2	4.54E-11
2015-06-15T08:41:31	2015-06-15T20:40:13	0	0	0
2015-06-15T22:21:17	2015-06-17T05:32:02	1	1	3.44E-12
2015-06-18T23:07:33	2015-06-20T05:55:15	2	2	3.73E-11
2015-06-20T07:36:31	2015-06-21T16:47:52	0	0	0
2015-06-21T18:29:52	2015-06-23T09:00:29	0	0	0
2015-06-23T10:41:59	2015-06-24T05:32:02	1	1	3.44E-12
2015-06-27T08:20:51	2015-07-01T05:32:02	7	7	1.98E-10
2015-07-03T01:34:12	2015-07-04T10:38:23	2	2	8.10E-10
2015-07-04T12:19:03	2015-07-06T09:15:15	13	1	4.24E-10
2015-07-06T10:55:59	2015-07-06T10:56:15	0	0	2.75E-11
2015-07-06T12:36:59	2015-07-08T05:32:04	8	8	9.12E-11
2015-07-09T23:16:49	2015-07-10T13:17:22	5	5	9.71E-11
2015-07-10T14:58:58	2015-07-11T16:28:13	1	1	9.73E-12
2015-07-11T18:09:43	2015-07-13T12:54:11	5	5	2.48E-10
2015-07-13T14:35:29	2015-07-15T05:32:03	3	3	2.11E-10
2015-07-17T19:42:41	2015-07-18T10:38:22	1	1	9.73E-12
2015-07-18T12:19:46	2015-07-19T06:44:43	8	8	2.13E-10
2015-07-19T08:26:31	2015-07-20T12:54:10	19	19	2.07E-10
2015-07-20T14:35:36	2015-07-21T09:00:31	19	19	3.39E-10
2015-07-21T10:34:41	2015-07-22T05:32:02	228	1	4.00E-09
2015-07-23T23:17:13	2015-07-24T13:07:14	0	0	0
2015-07-24T14:48:40	2015-07-24T16:06:30	0	0	0
2015-07-24T17:47:52	2015-07-25T10:38:23	5	5	9.24E-11
2015-07-25T12:19:39	2015-07-26T16:47:52	947	1	3.32E-08
2015-07-26T18:32:02	2015-07-27T12:54:11	23	23	3.44E-10
2015-07-27T14:38:19	2015-07-28T09:00:31	1	1	3.44E-12
2015-07-28T10:45:05	2015-07-29T05:32:02	4	4	7.45E-11
2015-07-31T14:30:51	2015-08-01T10:38:22	3803	1	4.68E-07
2015-08-01T12:37:08	2015-08-02T06:44:43	40	1	6.38E-10
2015-08-02T08:43:25	2015-08-03T12:54:10	71	71	1.03E-09

Table A1 – *continued*

Start date (YYYY-MM-DDThh:mm:ss)	End date (YYYY-MM-DDThh:mm:ss)	Number of fragments	Number of parents (3 per cent level of confidence)	Volume (m^3)
2015-08-03T14:52:46	2015-08-04T09:00:31	4	4	4.71E-11
2015-08-04T10:59:19	2015-08-05T05:32:02	41	1	5.97E-10
2015-08-06T18:18:17	2015-08-08T10:38:23	2	2	4.82E-11
2015-08-08T12:37:07	2015-08-09T06:44:42	1	1	2.75E-11
2015-08-09T08:43:36	2015-08-10T06:13:15	209	1	4.55E-09
2015-08-10T08:12:23	2015-08-10T22:57:19	1	1	2.75E-11
2015-08-11T00:56:38	2015-08-11T09:00:32	0	0	0
2015-08-11T10:59:50	2015-08-12T10:48:03	0	0	0
2015-08-14T14:45:25	2015-08-15T10:38:23	9	9	2.99E-10
2015-08-15T12:37:29	2015-08-16T06:44:42	1	1	2.75E-11
2015-08-16T08:44:02	2015-08-17T06:13:13	1	1	7.79E-11
2015-08-17T08:12:11	2015-08-17T22:57:19	1	1	9.73E-12
2015-08-18T00:56:12	2015-08-18T09:00:30	0	0	0
2015-08-18T10:59:24	2015-08-19T10:48:03	2	2	5.51E-11
2015-08-21T14:46:19	2015-08-22T10:38:24	27	27	2.00E-09
2015-08-22T12:37:28	2015-08-24T06:13:14	9	1	1.61E-10
2015-08-24T08:12:18	2015-08-24T22:57:18	1	1	3.08E-10
2015-08-25T00:56:23	2015-08-25T09:00:31	0	0	0
2015-08-25T10:59:35	2015-08-26T05:32:04	5	5	2.02E-10
2015-08-27T18:18:43	2015-08-29T10:38:23	66	1	1.69E-09
2015-08-29T12:38:53	2015-08-30T06:44:44	7	7	2.03E-10
2015-08-30T08:32:40	2015-08-31T12:54:13	8	8	2.40E-10
2015-08-31T14:41:53	2015-08-31T22:57:19	0	0	0
2015-09-01T00:45:20	2015-09-01T09:00:30	5	5	5.05E-11
2015-09-01T10:48:06	2015-09-02T15:44:55	5	5	1.43E-10
2015-09-04T06:51:51	2015-09-05T10:38:24	0	0	0
2015-09-05T12:26:04	2015-09-06T00:07:33	2	2	7.69E-11
2015-09-06T01:55:27	2015-09-06T05:04:45	0	0	0
2015-09-06T06:52:17	2015-09-08T09:00:30	53	1	1.23E-08
2015-09-08T10:48:38	2015-09-09T00:18:52	1	1	5.06E-11
2015-09-11T14:46:43	2015-09-12T13:29:58	8	1	2.92E-10
2015-09-12T15:29:00	2015-09-12T19:01:32	0	0	0
2015-09-12T21:00:30	2015-09-13T06:49:39	0	0	0
2015-09-13T08:57:59	2015-09-14T02:51:02	1	1	9.73E-12
2015-09-14T04:50:00	2015-09-15T09:00:31	0	0	0
2015-09-15T10:59:23	2015-09-16T15:44:56	21	21	3.48E-10
2015-09-18T04:32:05	2015-09-23T06:00:12	3	3	5.51E-11
2015-09-26T20:37:13	2015-09-30T05:32:02	8	1	2.14E-10
2015-10-02T20:04:18	2015-10-04T16:47:52	0	0	0
2015-10-04T18:45:26	2015-10-06T09:00:29	0	0	0
2015-10-06T10:58:25	2015-10-07T05:32:02	0	0	0
2015-10-11T07:37:01	2015-10-13T09:00:29	2	2	6.03E-11
2015-10-13T10:55:35	2015-10-14T05:55:12	0	0	0
2015-10-16T19:43:31	2015-10-18T16:47:52	1	1	2.75E-11
2015-10-18T18:42:58	2015-10-19T22:57:21	44	1	9.40E-10
2015-10-20T00:52:25	2015-10-21T05:55:12	0	0	0
2015-10-23T11:25:32	2015-10-29T22:23:27	315	1	1.22E-08
2015-10-31T06:30:22	2015-11-01T16:47:52	8	8	1.25E-10
2015-11-01T18:44:04	2015-11-02T22:57:21	10	1	1.40E-10
2015-11-03T00:53:37	2015-11-04T00:55:12	2	2	5.51E-11
2015-11-06T19:48:08	2015-11-07T05:55:13	0	0	0
2015-11-07T07:51:23	2015-11-09T01:00:13	1	1	1.43E-10
2015-11-09T02:56:21	2015-11-09T12:54:09	0	0	0
2015-11-09T14:50:19	2015-11-11T05:55:13	26	1	5.30E-10
2015-11-14T06:30:41	2015-11-16T00:31:01	1	1	1.79E-11
2015-11-16T02:27:11	2015-11-16T12:54:09	0	0	0
2015-11-16T14:50:27	2015-11-18T05:32:03	473	1	2.37E-08
2015-11-20T14:44:55	2015-11-22T23:30:12	124	1	2.68E-09
2015-11-23T01:28:29	2015-11-23T11:39:13	0	0	0
2015-11-23T13:37:15	2015-11-24T09:00:28	4	4	1.63E-10
2015-11-24T10:58:34	2015-11-24T23:30:12	1	1	2.75E-11
2015-11-27T14:43:57	2015-11-30T02:51:02	12	12	3.38E-10
2015-11-30T04:50:08	2015-11-30T12:54:10	0	0	0

Table A1 – *continued*

Start date (YYYY-MM-DDThh:mm:ss)	End date (YYYY-MM-DDThh:mm:ss)	Number of fragments	Number of parents (3 per cent level of confidence)	Volume (m^3)
2015-11-30T14:52:20	2015-12-01T09:00:31	0	0	0
2015-12-01T10:58:45	2015-12-02T00:00:17	0	0	0
2015-12-04T19:50:43	2015-12-06T06:44:41	4	1	2.96E-10
2015-12-06T08:43:05	2015-12-07T02:51:00	1	1	1.79E-11
2015-12-07T04:49:14	2015-12-08T11:30:13	1	1	1.79E-11
2015-12-08T13:28:27	2015-12-08T17:30:13	0	0	0
2015-12-08T19:28:19	2015-12-09T00:18:57	1	1	6.37E-11
2015-12-11T19:44:55	2015-12-13T06:44:41	2	2	3.10E-11
2015-12-13T08:42:59	2015-12-14T01:01:00	2	1	3.73E-11
2015-12-14T02:59:18	2015-12-14T11:45:14	0	0	0
2015-12-14T13:43:24	2015-12-15T01:15:15	0	0	0
2015-12-15T03:13:23	2015-12-15T08:00:15	0	0	0
2015-12-15T09:58:27	2015-12-16T00:00:17	2	2	7.81E-11
2015-12-18T19:45:00	2015-12-19T05:55:14	2	2	1.61E-09
2015-12-19T07:53:14	2015-12-20T06:44:41	1	1	9.29E-11
2015-12-20T08:42:55	2015-12-21T11:45:14	0	0	0
2015-12-21T13:43:44	2015-12-21T21:25:10	2	2	1.71E-10
2015-12-22T03:21:31	2015-12-22T08:00:13	0	0	0
2015-12-22T09:58:31	2015-12-23T00:00:11	2	2	6.03E-11
2015-12-25T19:51:04	2015-12-26T05:55:15	3	3	3.35E-10
2015-12-26T07:53:21	2015-12-27T06:44:42	24	1	4.64E-10
2015-12-27T08:43:02	2015-12-28T11:45:15	0	0	0
2015-12-28T13:43:35	2015-12-28T21:25:11	1	1	2.75E-11
2015-12-29T03:21:31	2015-12-29T08:00:15	0	0	0
2015-12-29T09:58:31	2015-12-30T00:00:17	1	1	1.79E-11
2016-01-01T19:46:36	2016-01-02T06:00:11	2	2	1.95E-11
2016-01-02T07:56:31	2016-01-03T06:49:40	0	0	0
2016-01-03T08:46:00	2016-01-04T00:51:03	0	0	0
2016-01-04T02:49:23	2016-01-04T11:30:15	0	0	0
2016-01-04T13:28:35	2016-01-05T11:30:14	0	0	0
2016-01-05T13:29:04	2016-01-06T00:00:16	0	0	0
2016-01-08T19:45:11	2016-01-09T06:00:10	1	1	2.75E-11
2016-01-09T07:56:32	2016-01-10T06:49:38	0	0	0
2016-01-10T08:45:58	2016-01-11T05:20:59	0	0	0
2016-01-11T07:19:21	2016-01-11T11:45:13	0	0	0
2016-01-11T13:43:21	2016-01-12T09:00:30	1	1	9.73E-12
2016-01-12T10:58:58	2016-01-13T00:18:57	0	0	0
2016-01-15T19:44:51	2016-01-16T06:00:10	0	0	0
2016-01-16T07:56:30	2016-01-17T06:49:39	0	0	0
2016-01-17T08:45:59	2016-01-18T05:21:00	4	4	8.54E-10
2016-01-18T07:19:02	2016-01-18T11:45:14	1	1	3.44E-12
2016-01-18T13:43:24	2016-01-19T09:00:30	0	0	0
2016-01-19T10:58:46	2016-01-20T00:00:16	0	0	0
2016-01-22T19:55:01	2016-01-23T05:55:14	0	0	0
2016-01-23T07:53:32	2016-01-24T06:44:43	2	2	1.02E-10
2016-01-24T08:42:59	2016-01-25T11:45:14	1	1	9.73E-12
2016-01-25T13:43:28	2016-01-26T09:00:31	519	1	2.02E-08
2016-01-26T11:00:25	2016-01-27T00:00:17	12	1	2.58E-10
2016-01-29T19:46:47	2016-01-30T05:55:14	1	1	9.73E-12
2016-01-30T07:54:58	2016-01-31T06:44:43	8	1	6.42E-11
2016-01-31T08:44:29	2016-02-01T11:45:14	13	13	2.68E-10
2016-02-01T13:45:02	2016-02-02T09:00:31	22	22	2.51E-10
2016-02-02T11:00:15	2016-02-03T00:00:17	0	0	0
2016-02-05T19:46:49	2016-02-06T05:55:14	12	1	3.58E-10
2016-02-06T07:55:06	2016-02-07T06:44:43	67	1	3.93E-09
2016-02-07T08:44:47	2016-02-08T11:30:14	4	4	5.04E-11
2016-02-08T13:30:04	2016-02-08T16:45:20	1	1	1.20E-10
2016-02-08T18:45:16	2016-02-10T05:32:03	12	1	5.79E-10
2016-02-10T17:53:59	2016-02-11T07:13:50	12	12	5.28E-10
2016-02-14T04:09:07	2016-02-15T11:30:14	0	0	0
2016-02-15T13:17:54	2016-02-15T16:45:20	15	15	3.06E-10
2016-02-15T18:45:06	2016-02-17T00:00:11	20	20	3.45E-10
2016-02-20T06:36:30	2016-02-21T06:44:41	8	8	1.92E-10

Table A1 – *continued*

Start date (YYYY-MM-DDThh:mm:ss)	End date (YYYY-MM-DDThh:mm:ss)	Number of fragments	Number of parents (3 per cent level of confidence)	Volume (m^3)
2016-02-21T08:06:07	2016-02-22T22:57:20	2	2	1.01E-10
2016-02-23T01:21:49	2016-02-24T00:18:58	1	1	2.75E-11
2016-02-27T06:36:31	2016-02-28T16:47:52	1	1	9.73E-12
2016-02-28T18:48:04	2016-02-29T12:54:11	3	3	5.64E-11
2016-02-29T14:54:29	2016-03-01T09:00:28	103	1	5.22E-08
2016-03-01T11:01:04	2016-03-02T08:12:03	12	12	1.05E-09
2016-03-04T16:59:17	2016-03-05T10:38:23	55	1	1.49E-09
2016-03-05T12:39:25	2016-03-06T06:44:42	2	2	1.52E-10
2016-03-06T08:45:34	2016-03-07T12:54:11	20	1	6.29E-10
2016-03-07T14:55:07	2016-03-08T09:00:30	0	0	0
2016-03-08T11:01:24	2016-03-09T00:00:12	0	0	0
2016-03-10T23:23:30	2016-03-12T05:55:14	9	1	8.42E-10
2016-03-12T07:37:16	2016-03-14T18:30:11	9	1	8.42E-10
2016-03-19T10:26:05	2016-03-21T02:50:13	18	18	2.28E-10
2016-03-21T04:50:27	2016-03-23T01:06:11	100	1	2.98E-09
2016-04-15T14:48:15	2016-04-17T16:47:53	0	0	0
2016-04-17T18:49:05	2016-04-20T05:32:03	2	2	5.64E-11
2016-04-23T16:04:00	2016-04-24T16:47:51	0	0	0
2016-04-24T18:48:45	2016-04-27T00:00:10	93	1	2.32E-09
2016-04-30T04:52:28	2016-05-01T05:55:15	0	0	0
2016-05-01T07:56:17	2016-05-03T09:00:30	0	0	0
2016-05-03T11:01:32	2016-05-04T00:00:16	3	3	9.35E-11
2016-05-07T04:52:30	2016-05-08T00:39:11	0	0	0
2016-05-10T19:41:03	2016-05-11T10:00:14	2	2	2.76E-11
2016-05-11T10:50:54	2016-05-11T20:15:14	0	0	0
2016-05-11T20:47:52	2016-05-12T06:25:15	49	1	1.46E-09
2016-05-12T07:16:13	2016-05-12T21:45:15	34	34	2.09E-09
2016-05-12T22:17:53	2016-05-13T08:00:14	14	1	2.06E-09
2016-05-13T08:50:58	2016-05-13T23:18:14	2	2	3.73E-11
2016-05-13T23:50:56	2016-05-14T09:35:15	0	0	0
2016-05-14T10:07:59	2016-05-14T23:18:35	20	20	9.54E-10
2016-05-15T00:09:43	2016-05-15T14:55:13	2	2	1.32E-11
2016-05-15T15:46:07	2016-05-15T19:45:13	0	0	0
2016-05-15T20:18:03	2016-05-16T05:30:14	0	0	0
2016-05-16T06:21:38	2016-05-16T20:10:14	1	1	2.75E-11
2016-05-16T20:42:56	2016-05-17T06:00:13	1	1	2.75E-11
2016-05-17T06:51:13	2016-05-17T15:45:15	2	2	1.28E-10
2016-05-17T16:17:59	2016-05-18T16:35:16	2	2	4.54E-11
2016-05-18T18:15:40	2016-05-18T22:00:14	0	0	0
2016-05-18T22:33:02	2016-05-19T02:10:14	0	0	0
2016-05-19T03:43:34	2016-05-19T22:30:13	258	1	3.53E-08
2016-05-19T23:03:09	2016-05-20T13:00:15	5	5	2.59E-10
2016-05-20T14:41:47	2016-05-20T18:30:15	0	0	0
2016-05-20T19:03:07	2016-05-21T05:00:15	0	0	0
2016-05-21T06:41:53	2016-05-21T23:15:34	2	2	1.56E-10
2016-05-21T23:48:28	2016-05-22T06:40:14	0	0	0
2016-05-22T07:13:04	2016-05-22T09:00:12	0	0	0
2016-05-22T09:33:02	2016-05-22T11:00:14	0	0	0
2016-05-22T11:33:04	2016-05-22T17:00:15	0	0	0
2016-05-22T18:34:25	2016-05-23T01:00:13	1	1	9.73E-12
2016-05-23T01:33:01	2016-05-23T11:00:15	2	1	3.58E-11
2016-05-23T12:41:59	2016-05-24T03:30:14	0	0	0
2016-05-24T04:03:06	2016-05-24T13:20:14	0	0	0
2016-05-24T15:02:00	2016-05-25T06:20:15	1	1	6.37E-11
2016-05-25T08:01:47	2016-05-27T08:00:15	4	4	1.09E-10
2016-05-27T09:41:57	2016-06-01T05:55:10	997	1	3.28E-08
2016-06-05T16:48:16	2016-06-06T02:10:29	2	2	1.20E-10
2016-06-06T03:04:19	2016-06-06T06:40:13	0	0	0
2016-06-06T08:24:45	2016-06-07T13:15:14	0	0	0
2016-06-07T14:55:26	2016-06-08T00:00:11	1	1	2.75E-11
2016-07-01T12:52:09	2016-07-07T07:13:45	188	1	7.64E-09
2016-07-07T10:40:55	2016-07-13T05:55:10	19	1	5.07E-09
2016-07-13T09:22:12	2016-07-16T20:41:30	11	1	4.80E-10

Table A1 *– continued*

Start date (YYYY-MM-DDThh:mm:ss)	End date (YYYY-MM-DDThh:mm:ss)	Number of fragments	Number of parents (3 per cent level of confidence)	Volume (m^3)
2016-07-17T00:08:54	2016-07-19T19:03:37	5	5	1.28E-09
2016-07-19T22:30:55	2016-07-22T12:45:12	0	0	2.75E-11
2016-07-23T16:07:32	2016-07-25T03:30:12	0	0	0
2016-07-25T06:57:46	2016-07-25T22:30:13	1	1	2.75E-11
2016-07-26T01:57:15	2016-07-26T09:30:27	0	0	0
2016-07-26T12:57:31	2016-07-26T23:30:12	2	2	1.05E-10
2016-07-27T02:57:24	2016-07-29T03:58:10	0	0	0
2016-07-29T07:16:36	2016-07-30T20:41:31	65	1	2.91E-09
2016-07-31T00:09:01	2016-08-02T09:30:27	3	1	4.32E-10
2016-08-02T12:57:47	2016-08-02T23:35:11	1	1	5.06E-11
2016-08-03T03:02:25	2016-08-04T17:26:37	0	0	0
2016-08-04T20:53:57	2016-08-06T01:35:12	2	2	3.10E-11
2016-08-06T05:02:27	2016-08-08T02:50:58	8	8	3.21E-10
2016-08-08T06:18:22	2016-08-09T23:25:11	0	0	0
2016-08-10T01:40:43	2016-08-11T20:00:11	5	5	2.10E-10
2016-08-11T23:27:33	2016-08-13T06:40:11	0	0	0
2016-08-15T05:22:35	2016-08-16T06:40:11	0	0	0
2016-08-17T01:57:49	2016-08-19T06:40:11	54	1	1.50E-09
2016-08-20T02:43:25	2016-08-22T07:17:13	2	2	1.32E-11
2016-08-23T02:47:29	2016-08-25T07:17:11	21	1	7.09E-10
2016-08-26T02:47:29	2016-08-28T07:17:13	12	1	3.17E-10
2016-08-29T02:47:29	2016-08-31T07:17:14	3	3	7.29E-11
2016-09-01T02:46:32	2016-09-03T07:17:12	6	6	8.60E-10
2016-09-05T05:20:14	2016-09-06T07:17:12	5223	1	2.52E-07
2016-09-11T06:04:13	2016-09-12T07:18:11	2	2	2.04E-09
2016-09-14T05:37:05	2016-09-15T07:17:15	4	4	7.09E-10
2016-09-17T05:35:35	2016-09-18T07:27:13	1	1	4.56E-10
2016-09-19T02:21:51	2016-09-19T18:07:05	0	0	0
2016-09-20T05:35:23	2016-09-21T07:17:11	0	0	0
2016-09-21T23:23:57	2016-09-22T17:30:41	0	0	0
2016-09-23T03:55:59	2016-09-24T07:17:11	0	0	0
2016-09-27T01:51:55	2016-09-27T14:08:11	1	1	5.06E-11

This paper has been typeset from a TEX/LATEX file prepared by the author.